Evolution of Pyrolysis Characteristics and Gas Components of Biochar Prepared by Either Mixing or Layering Rice Husk with Inert Aluminum Oxide

Wenfeng Liu,[a] Bichen Liu,[b] Yaohua Zhang,[a] Baojun Yi,[b] Hongyun Hu,[c] Qizhou Fan,[b] Chenqiao Li,[a] and Hui Liu [a,*]

A comparison of pyrolysis characteristics and gas product evolution of biochar with different packing arrangements was investigated. Pyrolysis properties and released gas products of rice husk char were obtained by particles in two different modes of packing. The results of the combustion characteristics of rice husk/char showed that the maximum pyrolysis rate of the rice husk decreased and the pyrolysis curve shifted to higher temperatures when the biomass was covered by Al_2O_3. The volatilization analysis of char from the covered biomass had a larger characteristic index and a lower activation energy. The 2D Fourier transform infrared (FTIR) results showed that layering hindered gaseous products from being released during rice husk pyrolysis, and there was no obvious release peak of C=O-containing organic matter. The 3D FTIR results showed that gaseous product absorption peak of solid product char pyrolysis gradually decreased while the rice husk conversion rate increased. The amount of H_2O, CO_2, CO, CH_4, and C=O-containing organic components released during combustion of pyrolyzed char when blended with Al_2O_3 decreased gradually. However, the pyrolysis gaseous product release was increased by the layering procedure.

DOI: 10.15376/biores.18.1.1699-1713

Keywords: Rice husk char; Pyrolysis; TGA-FTIR; Kinetics

Contact information: a: China Tobacco Hubei Industry Co., Ltd., Wuhan 430052, P. R. China; b: School of Engineering, Huazhong Agricultural University, Wuhan 430040, P. R. China; c: School of Energy and Power Engineering, Huazhong University of Science and Technology, Wuhan 430074, P. R. China;
** Corresponding author: liu_hui@hbtobacco.cn*

INTRODUCTION

Biomass thermochemical conversion technology (BTCT), as an important means to improve the utilization rate of biomass energy, has become a research hotspot in the field of clean energy. This technology is a promising technology for converting renewable biomass into bioenergy, biofuels, and special chemicals (Jha *et al.* 2022; Weir *et al.* 2022), which can partially replace fossil fuel utilization, alleviate environmental pollution, and solve other issues.

Biomass pyrolysis carbonization technology is the most basic heat treatment method for BTCT. Under the condition of thermal energy, a series of complex thermochemical transformations occur, mainly including devolatilization and carbonization. At present, traditional research on pyrolysis carbonization mainly focuses on biomass particle size (El Hanandeh *et al.* 2021), reactor (Soria-Verdugo *et al.* 2017), temperature (El Hanandeh *et al.* 2021), heating rate (Onsree *et al.* 2018), residence time (Wang *et al.* 2018b), solid heat carrier (Tan *et al.* 2018), and reaction atmosphere (Ma *et*

al. 2018), *etc.* However, biomass resources are diverse across the globe, and particle size is also different. Changes of the size and shape will change the bulk density of particle layer, and this will affect the heat and mass transfer rate between particles and char conversion during pyrolysis process, time, and char structure, *etc.* Therefore, it is necessary to explore the effects of different modes of biomass particles, such as their stacking in contrasting layers in preparation for the pyrolysis reaction processes. Current research is insufficient in this area. Some studies have only studied the association mechanism between particle size and pyrolysis product distribution (Wang *et al.* 2018a; Tabatabaei *et al.* 2019). Yu *et al.* (2018) used a fixed bed reactor to pyrolyze beech wood chips with three different particle sizes (0.21 to 0.50 mm, 0.85 to 1.70 mm, and 2.06 to 3.15 mm) to study the effect of particle size on pyrolysis char yield. The results showed that particle size mainly affects the pyrolysis reaction below 400 °C. As particle size increases, tar and gas yields decrease and char yields increase. Above 400 °C, a small particle size provides a larger surface area, resulting in tar cracking and condensation reactions becoming dominant, with similar char yields and increased gas yields. Di Blasi *et al.* (2013) pyrolyzed three particle sizes of beech wood particles (5 mm), crushed particles (1 to 25 mm), and ground particles (0.3 mm) in a packed bed. The heating rate and reaction temperature decreased with increasing particle bulk density in the range 0.3 to 0.6 g/cm^3; the char yields increased from 32.1% to 33.3%, and the carbon content increased from 71.6% to 72.4%. Soria-Verdugo *et al.* (2017) studied pyrolysis quality of sludge under different temperatures and airflow rates in fluidized bed and fixed bed reactors. It was found that the effect of temperature on pyrolysis is weaker than that of airflow velocity. Under a high airflow rate, the pyrolysis rate of sludge particles in the fluidized bed is higher than that in the fixed bed. In a fluidized bed reactor, the volatile substances released by sludge were about 53.4% at 500 °C, and about 60.1% at 600 °C. In a fixed bed reactor, the number of volatiles released by the sludge pyrolysis is decreased. In summary, it has been reported that the bulk density and packing state of particles significantly affect the heat and mass transfer, release of volatile gas products, and char yield in the pyrolysis of biomass particles. Meanwhile, the secondary reaction of volatile matter and char is increased.

Based on the condition, two kinds of packing arrangements were compared in this work for pyrolysis. One set of specimens was prepared by mixing biomass and Al_2O_3 (Azuara *et al.* 2015; Liu *et al.* 2019). Chattopadhyay *et al.* (2009) studied the Cu/Al_2O_3 catalyzed pyrolysis of biomass by thermogravimetric experiment, in which Al_2O_3 was used as the catalyst carrier. Sun *et al.* (2019) studied the effects of sludge ash, CaO, and Al_2O_3 on sludge pyrolysis and found that Al_2O_3 had little effect on pyrolysis carbon and gas. So Al_2O_3 can be regarded as only a bulk support material. It was found that the char prepared at low bulk density contains less O and H functional groups, and the char has good specific surface area and pore structure. High bulk density promotes the degree of aromatization of char, and char has good combustion reactivity; none of chars prepared at the target density reached a significant degree of graphitization (Liu *et al.* 2019). The mass transfer resistance will aggravate the secondary cracking reaction. In addition, the interaction between volatile matter and char will further promote the transformation of organic species released during pyrolysis (Zhou *et al.* 2014). The catalytic ability of char can promote the secondary pyrolysis of pyrolysis steam to form solid organic matter (Pattanotai *et al.* 2013; Hu *et al.* 2018). Based on current research, it is believed that the pyrolysis reaction is key to the pyrolysis process. Different char structure leads to the different pyrolysis reactivity.

Thermogravimetric and infrared spectroscopy (TGA-FTIR) not only can be used to study the weight loss law of substances during thermal decomposition, but it also can help

to identify the composition of pyrolysis gas and the changes in relative content in real time and online (Abdul Jameel *et al.* 2017; Müsellim *et al.* 2018). Parascanu *et al.* (2019) studied the pyrolysis of six biomass species. The results showed that the main gas products in volatile release stage of pyrolysis are H_2O, CO, CO_2, and CH_4 and organic compounds (aldehydes, ketones, and phenols). Ma *et al.* (2018) used TGA-FTIR to study the thermal degradation behavior of palm oil waste under nitrogen and air atmosphere, and they found that the main components in nitrogen atmosphere were CO_2, organic compounds with C=O bonds and organic compounds with C-H or C-O bonds, while it mainly released CO_2 and H_2O under air atmosphere. Therefore, rice husk chars were prepared at two packed modes using a fixed-bed pyrolysis reactor to improve the essence of pyrolysis mechanism under biomass particle stacking; the char reaction characteristic and gas release were studied *via* TGA-FTIR.

EXPERIMENTAL

Materials

Rice husk (RH), as a typical biomass, was selected for the experiment. The sample was crushed to the range of 100- to 200-mesh with a pulverizer and sieved to the range of 0.0750 to 0.150 mm. Al_2O_3 was selected with a particle size of 1 to 2 mm, heated in a muffle furnace at 800 °C for 3 h, and cooled for later use. The fine-particle Al_2O_3 was selected with a particle size of 100- to 200-mesh (analytical reagent, Sinopharm Chemical Reagent Co., Ltd., Shanghai, China), and dried in a drying oven at 105 °C for 24 h. The proximate analysis and elemental analysis calorific value of RH are shown in Table 1.

Table 1. Proximate Analysis, Elemental Analysis, and Calorific Value of RH

Sample	Proximate Analysis (wt%.ad)				Ultimate Analysis (wt%.daf)					LHV(MJ/kg)
RH	M	V	A	FC	C	H	O[a]	N	S	17.884
	8.03	67.20	9.66	15.11	55.19	6.93	37.08	0.35	0.46	

[a] Calculated by difference method

Note: ad- air-dry basis; daf- dry-free basis; M, moisture; V, volatile matter; A, ash; and FC, fixed carbon; LHV, lower heating value.

TGA-FTIR Characterization

First, (1 ± 0.1 g) RH and Al_2O_3 were mixed at a ratio of 1:10 using mixing mode and covering mode, respectively, and placed in a porcelain boat (100 × 40 × 20 mm^3). The mixing mode was as follows: Al_2O_3 and RH were placed in a centrifuge tube with setting proportion, shaken, and then poured into a porcelain boat to spread out. The covering mode was as follows: RH was added in the porcelain boat and spread out, and then Al_2O_3 was added in proportion to cover the RH evenly. When the furnace temperature reached 600 °C, high-purity nitrogen continued to aerate at 1 L/min, and the porcelain boat was quickly moved to the center of heating zone and the timer was started. After some reaction time, it was placed in a desiccator with nitrogen for complete cooling, weighing, recording, and then stored in a sample bag. Through several experiments to observe the weight loss of char during pyrolysis, the residence time of porcelain boat was determined at 2, 3, 4, 5, and 6 min (Liu *et al.* 2019). According to the experimental data of char and relative density among biochar, the mixing (or "blending") mode was labeled as RH-B-t; the covering mode was labeled as RH-C-t, where *t* stands for residence time. Default tests were carried out with rice husk alone (RH-t).

The TGA-FTIR utilized a thermogravimetric analyzer (TGA Q600, TA Instruments, New Castle, DE, USA) and a Fourier transform infrared spectrometer (Nicolet iS50, Thermo Fisher Scientific, Waltham, MA, USA). The initial mass of RH/RH char sample for each test was 5 mg, the flow rate of carrier gas was 100 mL/min nitrogen, and the temperature was raised from room temperature to 900 °C at a heating rate of 20 °C/min. The temperature of transmission line between TG and FTIR was mainly heated to 220 °C, and the absorption intensity of evolved gas was obtained online from FTIR. The resolution and spectral region of FTIR were 4 cm^{-1} and 4000 to 400 cm^{-1}, respectively. The spectral scanning time interval for 4 s. All samples were dried at 105 °C for 24 h, and then put it to TGA-FTIR experiments.

Pyrolysis Reaction Characteristic Index Analysis

The comprehensive release characteristic index (*D*) of volatiles was used to characterize the pyrolysis reaction characteristics of each sample. The calculation formula for the *D* value is as follows,

$$\boldsymbol{D} = \frac{(d\alpha/d\tau)_{\max}(d\alpha/d\tau)_{\text{mean}}}{t_s t_{\max} \Delta t_{1/2}} \quad (1)$$

where t_s is the initial precipitation temperature of volatiles (°C); t_{max} is the temperature of maximum weight loss rate (°C); $(d\alpha/d\tau)_{max}$ is the maximum weight loss rate (%/min); $(d\alpha/d\tau)_{mean}$ is the average weight loss rate (%/min); $\Delta t_{1/2}$ represents the temperature range of $(d\alpha/d\tau)/(d\alpha/d\tau)_{max}$ = 1/2 (°C). A larger value for *D* equates to better volatilization characteristics of the sample and an easier pyrolysis reaction.

Analysis of Kinetic Characteristics of RH Charcoal Pyrolysis

Biomass pyrolysis is a complex process because multiple reactions are involved. The straw pyrolysis kinetic model was based on the following assumption: A (solid) → B (char) + C (gas), where A is the solid material, B is the residual char after pyrolysis, and C is the pyrolysis gas product. The pyrolysis process of straw biochar is a typical heterogeneous solid-state reaction. In the thermogravimetric analysis of biomass heating weight loss process, the pyrolysis reaction kinetics can be described as,

$$\frac{d\alpha}{dt} = k \times f(\alpha) \quad (2)$$

where $\alpha = (m_0 - m) / (m_0 - m_\infty)$, is called the conversion rate, m_0 is the initial mass fraction of biomass (%), m_∞ is the remaining mass fraction of biomass (%), m is the pyrolysis mass fraction of the process (%), α_∞ is the conversion rate in the end (%), k is the reaction rate constant ($k = A\exp(-E/RT)$), where E is the apparent activation energy (kJ•mol^{-1}), R is the gas constant 8.314 × 10^{-3} (kJ /(mol•K), T is temperature (K), A is frequency factor (s^{-1}), $f(\alpha)$ is a function of conversion rate at α ($f(\alpha)=(1-\alpha)^n$), and n is reaction level number. After substituting $k = A\exp(-E/RT)$ and the heating rate $\beta = dT/dt$ into Eq. 2, one can obtain Eq. 3:

$$\frac{d\alpha}{f(\alpha)} = \frac{A}{\beta} exp\left(-\frac{E}{RT}\right) dT \quad (3)$$

The Coats-Redfern method has been widely used to treat kinetic parameters, such as *E* (Guo *et al.* 2018; Mian *et al.* 2019), pre-exponential factor, and reaction order, in biomass pyrolysis reaction kinetics at constant heating rate. Its formula is as follows:

$$ln\left(\frac{-ln(1-\alpha)}{T^2}\right) = ln\left[\frac{AR}{\beta E}\left(1-\frac{2RT}{E}\right)\right] - \frac{E}{RT} \text{ (n = 1)} \quad (4)$$

$$ln\left(\frac{-ln(1-\alpha)}{(1-n)T^2}\right) = ln\left[\frac{AR}{\beta E}\left(1-\frac{2RT}{E}\right)\right] - \frac{E}{RT} \text{ (n ≠ 1)} \quad (5)$$

The trial algorithm was used, and multiple different reaction orders (n = 0, 0.5, 1, 2, and 3) were assumed in the analysis process, and the correct reaction order was determined by the best fitting principle. The linear correlation of data is described by using the least squares method to calculate the fitting residuals. The degree of linearity is the highest when the reaction order n = 1. Therefore, when β remains unchanged, use $ln[-ln(1-\alpha)/T^2]$ as the ordinate and $1/T$ as the abscissa for fitting, $ln[-ln(1-\alpha)/T^2]$ and $1/T$ should be a fitted straight line, and the E can be obtained from the slope of straight line $-E/R$. Because $2RT/E<<1$, the intercept $ln[AR(1-2RT/E)/\beta E]$ can be regarded as a constant, and then A can be calculated from the intercept of fitting curve.

RESULTS AND DISCUSSION

Figure 1 shows the TG/DTG pyrolysis curves of RH under three conditions of packing, namely, the rice husk by itself, mixed with the Al_2O_3, and covered by the Al_2O_3, in the same amounts. Almeida *et al.* (2019) studied the three-component pyrolysis behavior of matter in a specific temperature range. The results showed that weight losses within the range 200 to 320 °C correspond to the decomposition of hemicellulose, 320 to 420 °C is for the decomposition of cellulose, and 420 to 700 °C is for the decomposition of lignin. Based on the DTG curve of RH without particle stacking in Fig. 1, RH pyrolysis can be divided into three categories: dehydration (30 to 119 °C), rapid devolatilization (182 to 417 °C), and carbonization (417 to 786 °C) stages. Most of the weight loss (86.8 wt%) of RH was associated with cracking into volatiles and char in the rapid devolatilization (182 to 417 °C) stage. The weight loss at this stage is mainly caused by the devolatilization of cellulose and hemicellulose, which is related to the temperature limit of thermal cracking of hemicellulose and cellulose. There is still a small part of weight loss (12.59 wt%) in the carbonization stage, which is mainly due to the pyrolysis of lignin and the continued devolatilization of char.

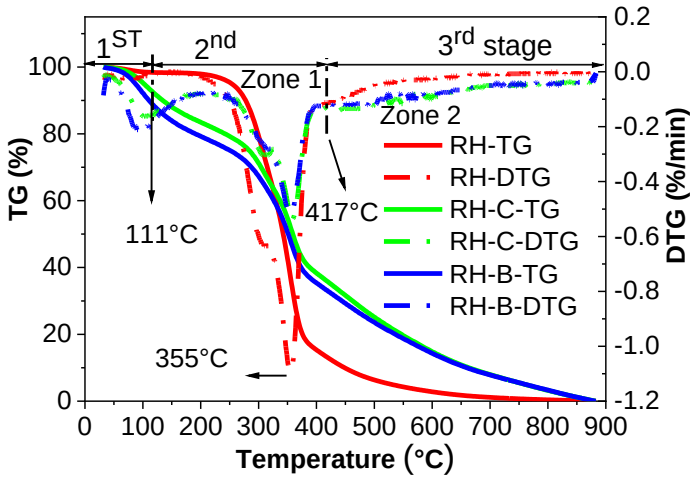

Fig. 1. TG/DTG pyrolysis curves of RH at three packing conditions

The TG/DTG pyrolysis curves of RH changed noticeably under different conditions of particle stacking. In the dehydration stage, water and volatile matter were released from RH particles, which may have increased the heat transfer caused by the addition of Al_2O_3. However, in the volatile phase, the α_∞ and $d\alpha/d\tau$ of RH decreased, $(d\alpha/d\tau)_{max}$ of pyrolysis decreased noticeably, and the $d\alpha/d\tau$ increased in the carbonization stage. The TG curves after 355 °C all shifted to the high temperature region, and the TG curves of RH samples prepared with covered biomass shifted more intensely. These findings show that the particles stacking with coverage by the Al_2O_3 mainly hindered the pyrolysis reaction in the stage of release volatiles and prolonged the conversion time of char in the carbonization stage.

Figure 2 shows the 2D FTIR map of RH pyrolysis at the first peak temperature (355 °C). Based on the infrared absorption bands in this 2D FTIR spectrum, some permanent gas components, such as H_2O, CH_4, CO_2, and CO, can be easily identified (Qiao *et al.* 2019). There was a stretching vibration peak of O-H bond at 3575 cm^{-1}, and the release of H_2O mainly came from the removal of O-H bond in the dehydration stage. At 2823 cm^{-1} was the stretching vibration of C-H bond, and the release of CH_4 was mainly the breaking of methoxy group (-OCH_3), methyl group (-CH_3-), and methylene group (-CH_2-). At 2308 cm^{-1} was the stretching vibration peak of carbonyl (C=O) and carboxyl (-COOH), and CO_2 mainly came from the decarboxylation and decarbonylation reactions in the devolatilization stage. The peak at 2178 cm^{-1} near the wavenumber 2308 cm^{-1} was the C-O bond stretching vibration, and the release of CO mainly came from the breaking of ether bonds (C-O-C) and C=O bonds. In addition to permanent gases, other components can be identified in wavenumbers 1800 to 1000 cm^{-1}, and the C=O stretching vibrational band at wavenumber 1770 cm^{-1} was attributed to aldehydes, ketones, and organic acids, which contains carbonyl groups (C=O-) and carboxyl group (-COOH). At the wavenumber of 1178 cm^{-1} were C-O, C-H bonds, and a carbon chain skeleton, containing alkanes, alcohols, ethers, and lipids.

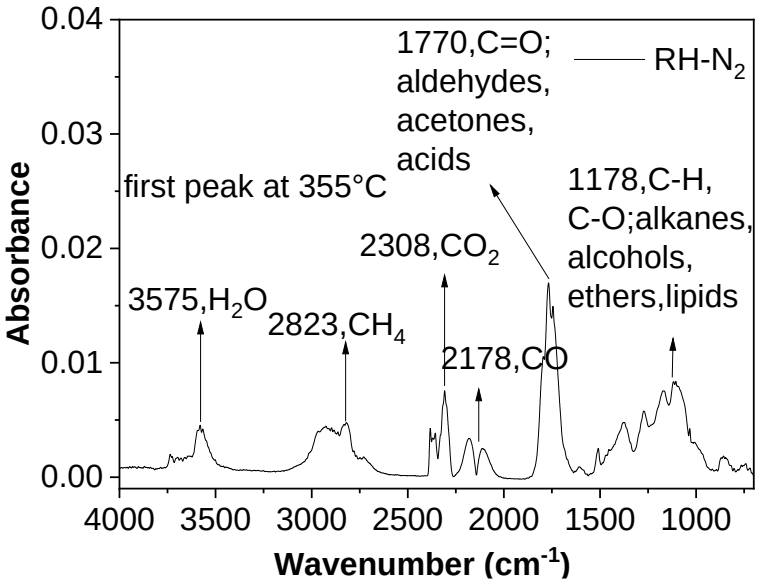

Fig. 2. 2D FTIR spectrum of RH pyrolysis under N_2 atmosphere at the first peak temperature (355 ^oC)

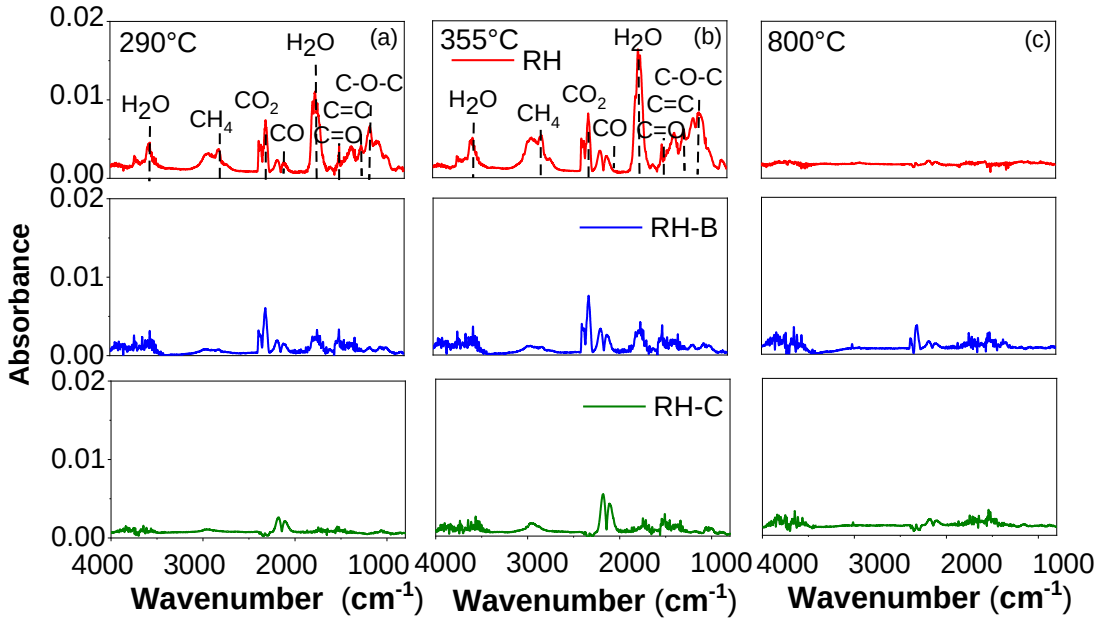

Fig. 3. 2D FTIR spectra of gas products of RH pyrolysis at three packing arrangements: (a) Start stage of pyrolysis; (b) pyrolysis stage at $(d\alpha/d\tau)_{max}$; (c) end stage of pyrolysis

Figure 3 shows the 2D FTIR spectra of the gas products of RH pyrolysis under three packing arrangements, 290 °C corresponds to the initial stage of pyrolysis, 355 °C corresponds to pyrolysis stage of $(d\alpha/d\tau)_{max}$, and 800 °C corresponds to the thermal solution end stage. The 290 °C spectrum mainly detected CO_2 and aldehydes or carboxylic acids containing C-O and C=O functional groups, as well as the release of a small amount of H_2O, CO, and CH_4. With the increase of the pyrolysis temperature, the release amount of each gas product in the 355 °C spectrum increased in a certain proportion compared with the 290 °C spectrum, and the proportion of release amount of CH_4 and aldehydes containing C-O functional groups increased remarkably. No substance was detected in the 800 °C spectrum, indicating the end of pyrolysis. Compared with the spectrum of raw RH without particle stacking, the absorbance peak intensity of each gas product in the spectrum of particle stacking pyrolysis (RH-B and RH-C) at 290 °C and 355 °C were noticeably reduced, and no functional group of aldehydes or carboxylic acids containing C-O or C=O were detected in the spectrum. The release peaks of each gas product from the pyrolysis of RH prepared with covered biomass were lower. The Al_2O_3 covering affects the distribution of gaseous products and hinders the release rate of gaseous products, which will increase the possibility of secondary reaction between volatiles and char.

Figure 4 shows the TG/DTG pyrolysis curves of RH char prepared with different residence times under the different packing arrangements. Because RH-B and RH-C pyrolysis was more than 4 min, most carbon had been completely reacted during biochar prepared processing. When biochar is pyrolyzed again, there's not much carbon to react. The structural change of char influences the pyrolysis reaction. As the residence time increased, the pyrolysis curve of char shifted to a higher temperature region and the weight loss of char gradually decreased. Meanwhile, the peak value of $(d\alpha/d\tau)_{max}$ of char gradually decreased. Under the same residence time, α_∞ and $(d\alpha/d\tau)_{max}$ of RH-C-t were both larger. However, the difference of α between RH-C and RH-B gradually decreased with increased residence time. The RH-B showed little resistance to the pyrolysis reaction, and a RH char easily released gaseous substances in the volatile release stage. The coverage of biomass

by Al_2O_3 hindered the pyrolysis reaction of particles, which increased the possibility of char secondary reaction, resulting in the release of volatiles mainly during the char pyrolysis process. As the residence time increased, the $d\alpha/d\tau$ value of RH char pyrolysis were close together, which resulted from the combined effect of atmosphere, temperature, and packing arrangement.

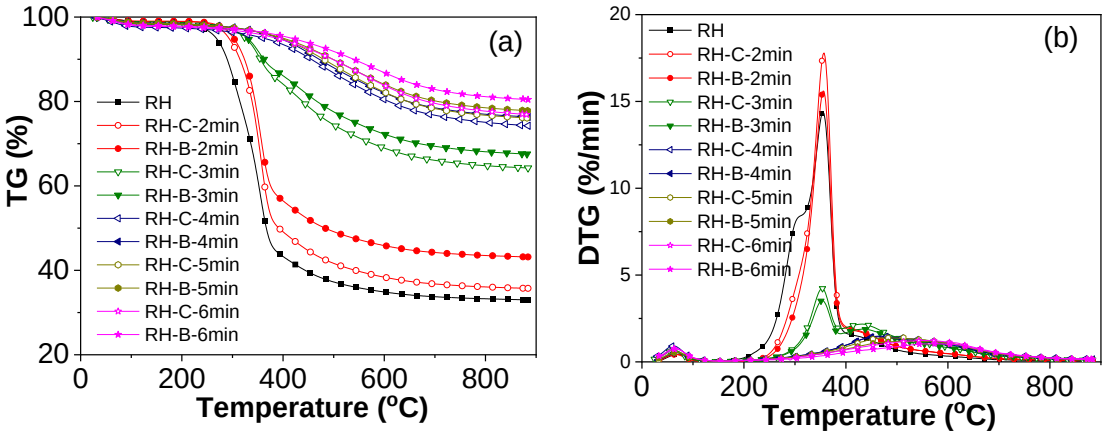

Fig. 4. TG/DTG pyrolysis curves of RH char prepared at different residence times, (a) TG and (b) DTG

Table 2 shows that with increased residence time, t_s and t_{max} gradually increased and $(d\alpha/d\tau)_{max}$, $(d\alpha/d\tau)_{mean}$, D, and α_∞ decreased gradually. Compared with the D value of RH-B-t, the D value of RH-C-t was larger, indicating that the char prepared with covered biomass was more favorable for pyrolysis.

Table 2. Pyrolysis Characteristic Parameters of RH Char

Sample	(t_s) °C	(t_{max}) °C	($\Delta t_{1/2}$) °C	$(d\alpha/d\tau)_{max}$ (%•min^{-1})	$(d\alpha/d\tau)_{mean}$ (%•min^{-1})	D × 10^{-8}	Total Weight Loss, (ω/%)
RH	213	355	87	14.34	1.57	343	67.03
RH-C-2min	244	357	52	17.69	1.50	585	64.22
RH-B-2min	245	355	50	15.42	1.33	470	56.83
RH-C-3min	261	353	189	4.29	0.82	20.3	35.33
RH-B-3min	269	351	207	3.57	0.76	13.8	32.35
RH-C-4min	269	366	237	1.49	0.60	3.81	25.48
RH-B-4min	274	462	253	1.44	0.55	2.47	23.56
RH-C-5min	272	480	254	1.38	0.56	2.31	23.56
RH-B-5min	274	534	260	1.19	0.52	1.62	22.32
RH-C-6min	274	552	251	1.23	0.46	1.49	22.85
RH-B-6min	277	577	249	1.03	0.45	1.17	19.51

Figure 5 shows the 3D FTIR images of RH char pyrolysis at various residence times. At residence time of 2 min, the 3D FTIR of char pyrolysis clearly shows the released gas product peaked at 3575, 2823, 2308, 2178, 1770, and 1178 cm^{-1}, corresponding to H_2O, CH_4, CO_2, CO, and organic compounds containing C=O, respectively. Each infrared absorbance peak was sharp, and the peak shape was similar to the DTG curve. As the

residence time increased, the peak of released gas product gradually disappeared, indicating that the particle stacking mainly affected the heat transfer and gas diffusion. Up to the reaction limit, the pyrolyzable components in char will be decomposed and continue to release gas.

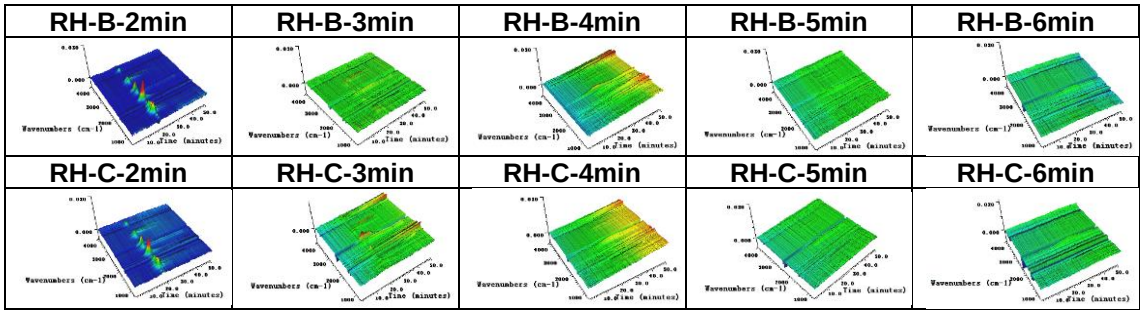

Fig. 5. 3D FTIR analysis of RH char prepared at different residence times

The release value is integral of all absorbance peaks of the same gas in the whole reaction process in Fig. 6. The release of H_2O can be attributed to the cleavage of O-H attached to the structure of cellulose and hemicellulose remaining in the char (Wang *et al.* 2011). From Fig. 6, The H_2O released decreased noticeably with increasing residence time. The release of H_2O mainly occurred in the early stage of RH pyrolysis, and minimal H_2O was released from char pyrolysis. The H_2O release value by the pyrolysis of RH-C char was higher than that of RH-B char, which can be attributed to the fact that the particles hinder the heat transfer between particles with covered biomass and increase the secondary reaction of volatiles with char, resulting in RH-C char that can release a higher content of O-H.

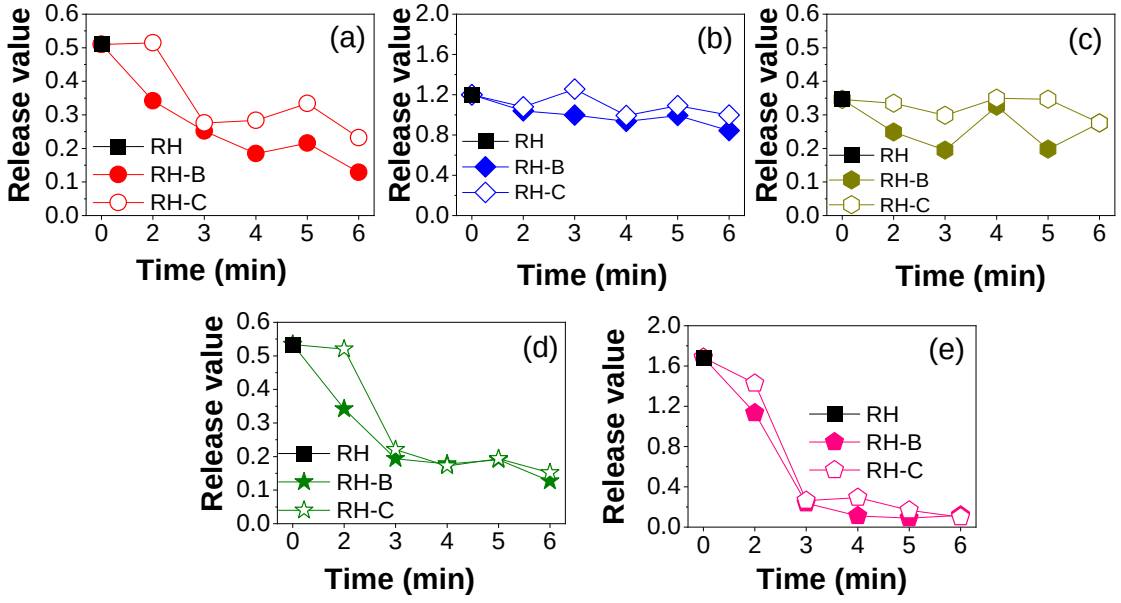

Fig. 6. Evolution of release of RH char pyrolysis gas products at different residence times, (a) H_2O, (b) CO_2, (c) CO, (d) CH_4, and (e) C=O contained organic components

The release of CO_2 is mainly caused by decarboxylation and decarbonylation reactions (Shen *et al.* 2010). The release amount of CO_2 decreases slowly with the increase of residence time. Coverage of the biomass hinders the cleavage of carboxyl and carbonyl groups in the volatiles/char, resulting in a higher CO_2 release from the pyrolysis of RH-C char. However, the particle packing density has little effect on the CO_2 release. This shows that the release pathway of CO_2 is not unique, involving mainly decarboxylation and decarbonylation reactions, but also involving the thermal release of other intermediates (such as aldehydes and propionic acid).

The CO formation pathway is caused by the cleavage of ether bonds (C-O-C) and the second cleavage or decarbonylation of aldehyde-containing intermediates, such as furfural, furan, and aldehyde (Ding *et al.* 2016). The release amount of CO decreases slowly with the increase of residence time, and the amount of CO released by pyrolysis of RH-C char is higher than that of RH-B char. This is like the CO_2 evolution condition. The release of CO mainly occurs in the second cracking or decarbonylation reaction of aldehyde-containing intermediates, such as furfural, furan, and aldehyde, and coverage of the biomass hinders the aldehyde-containing organics and decarbonylation reactions in the RH pyrolysis reaction.

CH_4 is mainly generated from the cleavage of three functional groups, namely methoxy ($-OCH_3$), methyl ($-CH_3$), and methylene ($-CH_2-$) (Meng *et al.* 2013). The released amount of CH_4 decreased remarkably with increased residence time, and the released amount of CH_4 from RH-C char was higher than that of RH-B char. This indicates that the release of CH_4 mainly occurred in the early of pyrolysis stage, and char pyrolysis could release little CH_4, and a coverage of the biomass hinders the thermal cracking reaction of $-OCH_3$, $-CH_3$, and $-CH_2-$ in RH pyrolysis.

The release of C=O organics is mainly due to the ring-opening reaction of the glucan unit in cellulose and the glycosyl unit in hemicellulose chain cleavage reaction (Yang *et al.* 2007). The evolution of C=O components is like that of CH_4, the release of C=O organics decreases noticeably with the increase of residence time, and the amount of C=O organics released by RH-C char pyrolysis is higher than that of RH-B Char. This shows that the release of C=O organic matter mainly occurs in the pyrolysis stage of RH, and the char contains minimal C=O organic matter. Coverage of the biomass by an inert material hinders the thermal cracking reaction of C=O organics in RH pyrolysis.

The value of *E* required for the pyrolysis of RH char varied with the conversion rate as shown in Fig. 7. According to the distribution of *E* of RH, the char pyrolysis process can be divided into four stages: (1) $0.1 < \alpha < 0.2$, hemicellulose pyrolysis stage; (2) $0.2 < \alpha < 0.4$, cellulose pyrolysis stage; (3) $0.4 < \alpha < 0.6$, lignin pyrolysis stage; and (4) $0.6 < \alpha < 0.8$, residual char pyrolysis stage. Stage (1): $0.1 < \alpha < 0.2$, the *E* was 69 to 79 kJ/mol, and the *E* increased in the initial stage. Yeo *et al.* (2019) proposed the mechanism of hemicellulose pyrolysis. Hemicellulose pyrolysis first undergoes branch chain breakage at a low temperature to obtain volatile products and intermediate products, and the degree of polymerization decreases. With the increase of pyrolysis temperature, the main chain of intermediate products depolymerization occurs, resulting in the production of various small molecular compounds, such as acetone, formic acid, formaldehyde, *etc.* Therefore, the *E* required for the reaction in the pyrolysis stage of hemicellulose is higher, and the *E* required for the pyrolysis reaction after the intermediate product is formed is lower. Stage (2): $0.2 < \alpha < 0.4$, the *E* was 61 to 79 kJ/mol, and the *E* gradually decreased. Chen *et al.* (2019) proposed that cellulose pyrolysis first produces an intermediate product, active cellulose, which reduces the degree of polymerization and the length of the molecular chain. After

that, as the temperature increases, the activated cellulose begins to crack. However, as the degree of polymerization decreases, pyrolysis is more likely to occur, so the *E* is lower than the initial stage. Stage (3): $0.4 < \alpha < 0.6$, the *E* is 61 to 85 kJ/mol, and the *E* gradually increases. Li *et al.* (2020) proposed the pyrolysis mechanism of lignin.

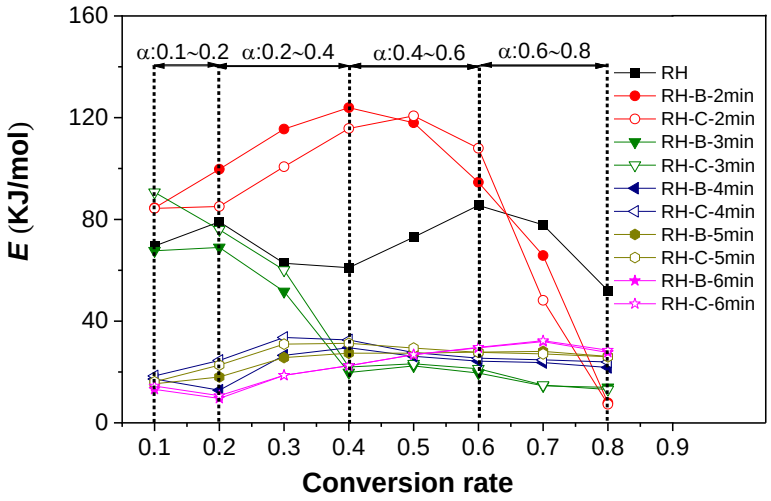

Fig. 7. Kinetic analysis of RH char pyrolysis

Lignin is mainly composed of three phenylpropane structures, which are closely combined with each other to form a three-dimensional network structure. Pyrolysis is the most difficult and requires the highest *E*. When α reached 0.6, the *E* increased suddenly and rapidly, which may be caused by the gradual increase in the content of char, the solid product of pyrolysis on the lignin surface. On the one hand, the reactivity of carbon is low. On the other hand, with the increase of temperature, the pyrolysis reaction mainly depends on the diffusion rate of the diffusion reaction zone. With the decrease of degradable substances, the reaction rate decreases sharply, resulting in a rapid increase in *E*. Stage (4) $0.6 < \alpha < 0.8$, the *E* was 52 to 85 kJ/mol, and the *E* decreased. At the end of pyrolysis, solid char forms a carbon skeleton through high temperature, and there are few thermally degradable products, so the *E* decreases.

As the residence time increased, the *E* of RH char pyrolysis decreased with conversion rate increase. Compared with the *E* required for the pyrolysis of the RH-B char, the value of *E* required for the pyrolysis of the RH-C char was smaller. This indicates that the coverage of the biomass by Al_2O_3 hinders heat transfer and volatile diffusion of RH, increases the thermal conversion time between particles, and results in a high content of organic components in the prepared char.

CONCLUSIONS

1. Particle stacking mainly affected the pyrolysis reaction of RH in the volatile release stage, and it noticeably affected the release rate and product distribution of gaseous substances. Coverage of the RH with Al_2O_3 led to the decrease of the maximum weight loss rate RH pyrolysis, and the pyrolysis curve shifted to a higher temperature region.

2. The initial volatile precipitation temperature and maximum weight loss rate temperature of char increased gradually with the increase of char residence time, while the maximum weight loss rate, average weight loss rate, volatile comprehensive release characteristic index, and total weight loss rate gradually decreased. The volatilization characteristics of char prepared with coverage of the biomass by Al_2O_3 were stronger, and the pyrolysis reaction required a smaller activation energy.
3. The absorbance peak value of char pyrolysis gas products gradually decreased, and this evolution shape was similar to the DTG curve, in which the release amount of H_2O, CO_2, CO, CH_4, and organic components containing C=O increased with the residence time of char pyrolysis and then gradually decreased. The char pyrolysis gas product produced with a coverage of the biomass by Al_2O_3 had a higher release amount.

ACKNOWLEDGMENTS

This work was supported by support enterprise technology innovation and development projects (2021BAB115) and the Key Research and Development Program of Hubei Provincial (2021BBA226). The authors also acknowledge the extended help from the Analytical and Testing Center of Huazhong Agricultural University (HZAU).

REFERENCES CITED

Abdul Jameel, A. G., Han, Y., Brignoli, O., Telalović, S., Elbaz, A. M., Im, H. G., Roberts, W. L., and Sarathy, S. M. (2017). "Heavy fuel oil pyrolysis and combustion: Kinetics and evolved gases investigated by TGA-FTIR," *Journal of Analytical and Applied Pyrolysis* 127, 183-195. DOI: 10.1016/j.jaap.2017.08.008

Almeida, S. R., Elicker, C., Vieira, B. M., Cabral, T. H., Silva, A. F., Sanches Filho, P. J., Raubach, C. W., Hartwig, C. A., Mesko, M. F., Moreira, M. L., *et al.* (2019). "Black SiO_2 nanoparticles obtained by pyrolysis of rice husk," *Dyes and Pigments* 164, 272-278. DOI: 10.1016/j.dyepig.2019.01.030

Azuara, M., Fonts, I., Bimbela, F., Murillo, M. B., and Gea, G. (2015). "Catalytic post-treatment of the vapors from sewage sludge pyrolysis by means of γ-Al_2O_3: Effect on the liquid product properties," *Fuel Processing Technology* 130, 252-262. DOI: 10.1016/j.fuproc.2014.10.014

Chattopadhyay, J., Kim, C., Kim, R., and Pak, D. (2009). "Thermogravimetric study on pyrolysis of biomass with Cu/Al_2O_3 catalysts, " *Journal of Industrial and Engineering Chemistry* 15(1), 72-76. DOI: 10.1016/j.jiec.2008.08.022

Chen, L., Liao, Y., Guo, Z., Cao, Y., and Ma, X. (2019). "Products distribution and generation pathway of cellulose pyrolysis," *Journal of Cleaner Production* 232, 1309-1320. DOI: 10.1016/j.jclepro.2019.06.026

Di Blasi, C., Branca, C., Lombardi, V., Ciappa, P., and Di Giacomo, C. (2013). "Effects of particle size and density on the packed-bed pyrolysis of wood," *Energy & Fuels* 27(11), 6781-6791. DOI: 10.1021/ef401481j

Ding, Y., Ezekoye, O. A., Lu, S., and Wang, C. (2016). "Thermal degradation of beech wood with thermogravimetry/Fourier transform infrared analysis," *Energy Conversion and Management* 120, 370-377. DOI: 10.1016/j.enconman.2016.05.007

El Hanandeh, A., Albalasmeh, A., and Gharaibeh, M. (2021). "Effect of pyrolysis temperature and biomass particle size on the heating value of biocoal and optimization using response surface methodology," *Biomass and Bioenergy* 151, article 106163. DOI: 10.1016/j.biombioe.2021.106163

Guo, L., Zhai, M., Wang, Z., Zhang, Y., and Dong, P. (2018). "Comprehensive coal quality index for evaluation of coal agglomeration characteristics," *Fuel* 231, 379-386. DOI: 10.1016/j.fuel.2018.05.119

Hu, C., Zhang, H., and Xiao, R. (2018). "Effects of nascent char on ex-situ catalytic fast pyrolysis of wheat straw," *Energy Conversion and Management* 177, 765-772. DOI: 10.1016/j.enconman.2018.10.018

Jha, S., Okolie, J. A., Nanda, S., and Dalai, A. K. (2022). "A review of biomass resources and thermochemical conversion technologies," *Chemical Engineering & Technology* 45(5), 791-799. DOI: 10.1002/ceat.202100503

Li, J., Bai, X., Fang, Y., Chen, Y., Wang, X., Chen, H., and Yang, H. (2020). "Comprehensive mechanism of initial stage for lignin pyrolysis," *Combustion and Flame* 215, 1-9. DOI: 10.1016/j.combustflame.2020.01.016

Liu, B., Fan, Q., Wu, W., and Hu, Y. (2019). "Structure and reactivity of rice husk chars under different bulk densities," *BioResources* 14(4), 8289-8303. DOI: 10.15376/biores.14.4.8289-8303

Ma, Z., Wang, J., Yang, Y., Zhang, Y., Zhao, C., Yu, Y., and Wang, S. (2018). "Comparison of the thermal degradation behaviors and kinetics of palm oil waste under nitrogen and air atmosphere in TGA-FTIR with a complementary use of model-free and model-fitting approaches," *Journal of Analytical and Applied Pyrolysis* 134, 12-24. DOI: 10.1016/j.jaap.2018.04.002

Meng, A., Zhou, H., Qin, L., Zhang, Y., and Li, Q. (2013). "Quantitative and kinetic TG-FTIR investigation on three kinds of biomass pyrolysis," *Journal of Analytical and Applied Pyrolysis* 104, 28-37. DOI: 10.1016/j.jaap.2013.09.013

Mian, I., Li, X., Jian, Y., Dacres, O. D., Zhong, M., Liu, J., Ma, F., and Rahman, N. (2019). "Kinetic study of biomass pellet pyrolysis by using distributed activation energy model and Coats Redfern methods and their comparison," *Bioresource Technology* 294, article ID 122099. DOI: 10.1016/j.biortech.2019.122099

Müsellim, E., Tahir, M. H., Ahmad, M. S., and Ceylan, S. (2018). "Thermokinetic and TG/DSC-FTIR study of pea waste biomass pyrolysis," *Applied Thermal Engineering* 137, 54-61. DOI: 10.1016/j.applthermaleng.2018.03.050

Onsree, T., Tippayawong, N., Zheng, A., and Li, H. (2018). "Pyrolysis behavior and kinetics of corn residue pellets and eucalyptus wood chips in a macro thermogravimetric analyzer," *Case Studies in Thermal Engineering* 12, 546-556. DOI: 10.1016/j.csite.2018.07.011

Parascanu, M. M., Sánchez, P., Soreanu, G., Valverde, J. L., and Sanchez-Silva, L. (2019). "Mexican biomasses valorization through pyrolysis process: Environmental and costs analysis," *Waste Management* 95, 171-181. DOI: 10.1016/j.wasman.2019.06.007

Pattanotai, T., Watanabe, H., and Okazaki, K. (2013). "Experimental investigation of intraparticle secondary reactions of tar during wood pyrolysis," *Fuel* 104, 468-475. DOI: 10.1016/j.fuel.2012.08.047

Qiao, Y., Wang, B., Zong, P., Tian, Y., Xu, F., Li, D., Li, F., and Tian, Y. (2019). "Thermal behavior, kinetics and fast pyrolysis characteristics of palm oil: Analytical TG-FTIR and Py-GC/MS study," *Energy Conversion and Management* 199, article ID 111964. DOI: 10.1016/j.enconman.2019.111964

Shen, D. K., Gu, S., and Bridgwater, A. V. (2010). "Study on the pyrolytic behaviour of xylan-based hemicellulose using TG–FTIR and Py–GC–FTIR," *Journal of Analytical and Applied Pyrolysis* 87(2), 199-206. DOI: 10.1016/j.jaap.2009.12.001

Soria-Verdugo, A., Morato-Godino, A., Garcia-Gutierrez, L. M., and Garcia-Hernando, N. (2017). "Pyrolysis of sewage sludge in a fixed and a bubbling fluidized bed – Estimation and experimental validation of the pyrolysis time," *Energy Conversion and Management* 144, 235-242. DOI: 10.1016/j.enconman.2017.04.062

Sun, Y., Chen, J., and Zhang, Z. (2019). "General roles of sludge ash, CaO and Al_2O_3 on the sludge pyrolysis toward clean utilizations, " *Applied Energy* 233-234, 412-423. DOI: 10.1016/j.apenergy.2018.10.034

Tabatabaei, M., Aghbashlo, M., Dehhaghi, M., Panahi, H. K. S., Mollahosseini, A., Hosseini, M., and Soufiyan, M. M. (2019). "Reactor technologies for biodiesel production and processing: A review," *Progress in Energy and Combustion Science* 74, 239-303. DOI: 10.1016/j.pecs.2019.06.001

Tan, Y. L., Abdullah, A. Z., and Hameed, B. H. (2018). "Catalytic fast pyrolysis of durian rind using silica-alumina catalyst: Effects of pyrolysis parameters," *Bioresource Technology* 264, 198-205. DOI: 10.1016/j.biortech.2018.05.058

Wang, S., Guo, X., Wang, K., and Luo, Z. (2011). "Influence of the interaction of components on the pyrolysis behavior of biomass," *Journal of Analytical and Applied Pyrolysis* 91(1), 183-189. DOI: 10.1016/j.jaap.2011.02.006

Wang, T., Zhai, Y., Zhu, Y., Li, C., and Zeng, G. (2018a). "A review of the hydrothermal carbonization of biomass waste for hydrochar formation: Process conditions, fundamentals, and physicochemical properties," *Renewable and Sustainable Energy Reviews* 90, 223-247. DOI: 10.1016/j.rser.2018.03.071

Wang, X., Bai, S., Jin, Q., Li, S., Li, Y., Li, Y., and Tan, H. (2018b). "Soot formation during biomass pyrolysis: Effects of temperature, water-leaching, and gas-phase residence time," *Journal of Analytical and Applied Pyrolysis* 134, 484-494. DOI: 10.1016/j.jaap.2018.07.015

Weir, A., Jiménez del Barco Carrión, A., Queffélec, C., Bujoli, B., Chailleux, E., Uguna, C. N., Snape, C., and Airey, G. (2022). "Renewable binders from waste biomass for road construction: A review on thermochemical conversion technologies and current developments," *Construction and Building Materials* 330, article ID 127076. DOI: 10.1016/j.conbuildmat.2022.127076

Yang, H., Yan, R., Chen, H., Lee, D. H., and Zheng, C. (2007). "Characteristics of hemicellulose, cellulose and lignin pyrolysis," *Fuel* 86(12), 1781-1788. DOI: 10.1016/j.fuel.2006.12.013

Yeo, J. Y., Chin, B. L. F., Tan, J. K., and Loh, Y. S. (2019). "Comparative studies on the pyrolysis of cellulose, hemicellulose, and lignin based on combined kinetics," *Journal of the Energy Institute* 92(1), 27-37. DOI: 10.1016/j.joei.2017.12.003

Yu, J., Sun, L., Berrueco, C., Fidalgo, B., Paterson, N., and Millan, M. (2018). "Influence of temperature and particle size on structural characteristics of chars from beechwood pyrolysis," *Journal of Analytical and Applied Pyrolysis* 130, 127-134. DOI: 10.1016/j.jaap.2018.01.018

Zhou, S., Garcia-Perez, M., Pecha, B., McDonald, A., and Westerhof, R. (2014). "Effect of particle size on the composition of lignin derived oligomers obtained by fast pyrolysis of beech wood," *Fuel* 125, 15-19. DOI: 10.1016/j.fuel.2014.01.016

Article submitted: June 8, 2022; Peer review completed: December 31, 2022; Revised version received and accepted: January 9, 2023; Published: January 13, 2023.
DOI: 10.15376/biores.18.1.1699-1713